Devil's staircase magnetic spirals in $Ni_{2-x}Co_xScSbO_6$

Kunlang Ji [1,*] Elena Solana-Madruga [2] Angel M. Arevalo-Lopez [3] Pascal Manuel,[4] and J. Paul Attfield [1,†]

[1]*Centre for Science at Extreme Conditions and School of Chemistry, University of Edinburgh, United Kingdom*

[2]*Dpto. Q. Inorgánica, Universidad Complutense de Madrid, Avda. Complutense sn, Madrid 28040, Spain*

[3]*Université Lille, CNRS, Centrale Lille, ENSCL, Université Artois, UMR 8181–UCCS–Unité de Catalyse et Chimie du Solide, Lille F-59000, France*

[4]*ISIS, Rutherford Appleton Laboratory, Harwell Oxford, Didcot OX11 0QX, United Kingdom*

(Received 5 January 2026; revised 28 April 2026; accepted 5 June 2026; published 6 July 2026)

$Ni_{2-x}Co_xScSbO_6$ solid solutions ($x = 0.1$, 0.2, 0.3, 0.4) have been studied by magnetization and neutron powder diffraction measurements. All samples are magnetically ordered below $T_C \approx 63$ K and metamagnetic transitions are observed at fields ~ 2.5 T at 2 K. Neutron diffraction shows that the metamagnetic transition marks a k-flop from helical wave vector $\boldsymbol{k} = [0\,0\,k_z]$ to cycloidal $\boldsymbol{k} = [k_x\,0\,0]$ spin spirals, and the latter gradually transform to a coexisting ferrimagnetic $\boldsymbol{k} = [0\,0\,0]$ state at higher field. Fractional values of k_z and k_x are consistent with complete devil's staircase behavior, driven by locking-in of spins to easy-axis directions in the ab-plane that stabilizes commensurate $6p/q$ wave vectors (p, q = integers).

DOI: 10.1103/dlvy-9bd9

I. INTRODUCTION

Complex magnetic structures are of interest as frustrated systems and for coupling of magnetism to lattice distortions which can give rise to multiferroics, where electrical and magnetic polarization coexist [1–3]. Spiral magnetic structures are found in many frustrated systems, and when wave vector varies with tuning parameter then the series of observed fractional commensurate and incommensurate states may follow proposed devil's and other staircase models [4]. Famous examples are in simple rare earth metals or alloys such as Ho metal [5] and CeSb, with the latter showing at least seven fractional commensurate superstructures as a function of temperature [6].

Chemically-tunable commensurate helical spin structures were recently reported in a series of complex, disordered transition metal oxides — Ni_3TeO_6 (NTO) type solid solutions $Ni_{2-x}Co_xScSbO_6$ [7]. NTO types are an important family of materials derived from the corundum (Al_2O_3) structure, where cation ordering can induce electrical polarization by lowering symmetry from centric $R\bar{3}c$ in corundum to polar $R3c$ in $LiNbO_3$, and further to polar $R3$ in Ni_3TeO_6 (NTO) [8–11]. In such polar magnets, noncollinear spin structures can in principle couple to the lattice polarization and give rise to magnetoelectric effects, although the existence and magnitude of such coupling are strongly material dependent and require direct experiment verification. The symmetry-lowering in the NTO structure results in four distinct octahedral cation sites, one of which is typically occupied by a high valent nonmagnetic cation such as Nb^{5+}, Sb^{5+}, Te^{6+} or W^{6+} while divalent or trivalent transition metal cations with unpaired spins can locate at the other three [12–14]. Magnetic frustration arising from exchange interactions within and between triangular layers of spins can give rise to spiral spin structures and multiferroic properties through coupling to the structural polarization [15–20]. Mn_2MnWO_6 was found to have a large magnetoelectric effect where ferroelectricity was induced by magnetic ordering [21].

Ni_2ScSbO_6 was previously reported as an NTO type oxide that is ferroelectric below 1050 K and shows a low temperature helimagnetic spin structure with propagation wave vector $\boldsymbol{k} = [0\,0.036\,0]$ [18]. While the coexistence of structural polarity and noncollinear magnetic order in this compound permits magnetoelectric coupling by symmetry, no change of polarization associated with the helimagnetic ordering has yet been experimentally reported for Ni_2ScSbO_6. An investigation of Co-substituted variants found that a series of NTO-type solid solutions $Ni_{2-x}Co_xScSbO_6$ [Fig. 1(a)] can be prepared with magnetic transitions near $T_C \approx 60$ K [7]. Samples with $x = 0.5$, 1.0, 1.5 and 2.0 were all found to have long-period helical $[0\,0\,k_z]$ commensurate magnetic structures [Fig. 1(b)] with spins in the ab-plane and k_z values taking fractional $1/3n$ values for $n = 5$, 6, 8 and 10 respectively. This lock-in behavior is likely driven by the strong electronic anisotropy of Co^{2+}, arising from its unquenched orbital contribution, which favors the commensurate states where spins can lie parallel to easy-axes that have a 3-fold symmetry in the ab-plane of the $R3$ crystal structure [7]. For $x = 1.5$ and 2.0 samples, the helical spin structure coexists with a commensurate ferrimagnetic structure ($\boldsymbol{k} = [0\,0\,0]$) with collinear spin ordering in the ab-

*Current address: Institute for Chemical Research, Kyoto University, Gokasho, Uji, Kyoto 611-0011, Japan.

†Contact author: j.p.attfield@ed.ac.uk

Published by the American Physical Society under the terms of the Creative Commons Attribution 4.0 International license. Further distribution of this work must maintain attribution to the author(s) and the published article's title, journal citation, and DOI.

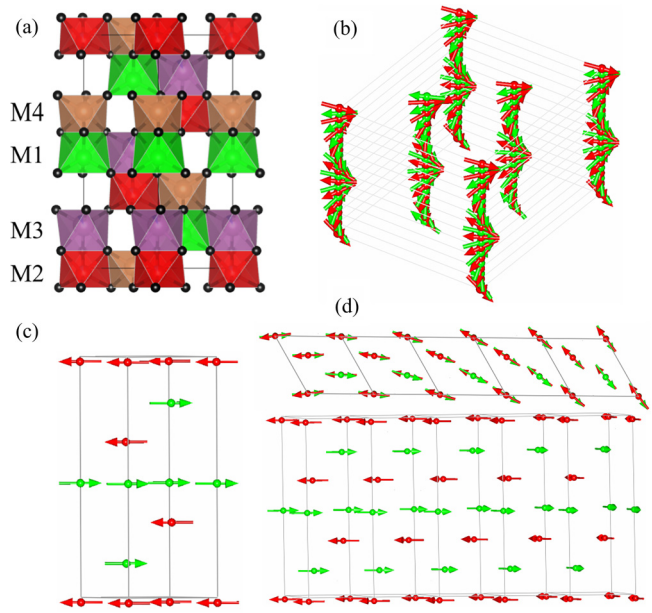


FIG. 1. (a) Crystal structure for $Ni_{2-x}Co_xScSbO_6$ solid solutions showing the four independent cation sites. (b) to (d) show the ordered M1 (green) and M2 (red) spins for (b) helical [0 0 k_z], (c) ferrimagnetic [000], and (d) cycloidal [k_x 0 0] magnetic structures. *R*3 unit cells are shown with the *c*-axis vertical in (a), (c) and (d). An *ab*-plane projection is also shown in (d).

plane [Fig. 1(c)]. The $x = 0.5$ sample shows metamagnetism with a critical field of $H_c = 1.5$ T at 4 K.

In the present study we have investigated $Ni_{2-x}Co_xScSbO_6$ samples for small Co contents ($x = 0.1$, 0.2, 0.3 and 0.4). This end of the series is of interest as lock-in effects are expected to be weaker when electronically anisotropic Co^{2+} is diluted by the more isotropic Ni^{2+}. Our magnetization and neutron scattering results show that helical [0 0 k_z] spin structures persist down to $x = 0.1$ but do not follow $1/3n$ values although they may be interpreted in terms of other fractional behavior. We have also discovered that the metamagnetic transition corresponds to a change in spin ordering from a helical [0 0 k_z] to a cycloidal [k_x 0 0] magnetic structure [Fig. 1(d)] where spins remain in the *ab*-plane. Evidence for field-tunable devil's staircase behavior is observed as k_x takes $1/3n$ values, although the cycloidal phase gradually converts to the ferrimagnetic [0 0 0] state at higher fields.

II. METHODS

Polycrystalline samples of $Ni_{2-x}Co_xScSbO_6$ ($x = 0.1$, 0.2, 0.3 and 0.4) were synthesized following a standard solid-state method. Stoichiometric proportions of NiO, CoO, Sc_2O_3 and Sb_2O_5 oxides were well mixed and sintered at 1473 K for 15 h. Several cycles of heating treatments at 1473 K were used to minimize secondary phases.

X-ray powder diffraction (XPD) was performed on a D2 Bruker X-ray diffractometer with Cu K_α radiation. Data for Rietveld refinement were collected at room temperature in the 2θ range $10-70^\circ$ with a step size of 0.1 and counting time 2s per step.

Magnetic susceptibility measurements were performed using Quantum Design MPMS and PPMS instruments. Zero-Field-Cooled (ZFC) and Field-Cooled (FC) data were collected over the temperature range $2 < T < 300$ K under magnetic fields of 0.01, 0.1, and 1 T. Magnetization (M) - field (H) loops were measured at 2 to 80 K.

Neutron powder diffraction (NPD) data were collected on the WISH diffractometer (ISIS, UK) for all $Ni_{2-x}Co_xScSbO_6$ samples ($x = 0.1$, 0.2, 0.3, and 0.4) at several temperatures between 1.7 and 100 K. 2 g powder samples were placed in 6 mm diameter vanadium cans and loaded into a helium cryostat. High magnetic field NPD measurements were carried also out on $x = 0.1$ and 0.2 samples using the GEM instrument magnet to collect data at 1.5 and 30 K under fields between 0 and 6 T. For these measurements, approximately 1.5 g of powder was pressed into a cylindrical pellet ($\sim$ 5 mm diameter, $\sim$ 10 mm height) and loaded into a vanadium can.

Rietveld analysis of XPD and NPD data was carried out using the FullProf software package [22]. Magnetic symmetry analysis on low temperature neutron data was performed by means of the BasIreps program [23].

III. RESULTS

A. Structural characterization

Sample color gradually changes from light to dark green with increasing cobalt content. Rietveld fits to room temperature XPD data (Fig. S1 [24]) show that NTO type $Ni_{2-x}Co_xScSbO_6$ phases are formed with >95% purity along with small amounts of secondary phases [rocksalt type (Co,Ni)O and $Sc_{5.5}Sb_{1.5}O_{12}$]. Lattice parameters and volumes are shown in Table S1. Representative values are $a = 5.17650(5)$ and $c = 14.0265(2)$ Å for $x = 0.1$. Plots in Fig. S2 show that lattice parameters increase monotonically with Co content x, as Co^{2+} (six-coordinate ionic radius 0.745 Å) is slightly larger than Ni^{2+} (0.69 Å).

NPD data collected at 100 K, well above the magnetic transition ($T_C \approx 63$ K), were used for nuclear structure refinements. The coherent neutron scattering lengths (b) of the four metals differ widely ($b_{Ni} = 10.3$, $b_{Co} = 2.49$, $b_{Sc} = 12.29$, and $b_{Sb} = 5.57$ fm) giving high contrast to determine the cation distribution over the four sites, and NPD also gives precise oxygen positions ($b_O = 5.803$ fm). Rietveld fits are shown in Fig. S3 [24]. In keeping with the previous study [18], it was found that site M1 is occupied by Ni/Co, M2 by Ni/Sc, M3 by Sc/Co, and M4 is fully occupied by Sb. Refinement results are in Table S1 and derived bond lengths, angles and bond valence sum (BVS) calculations are in Table S2 [24]. The BVS's are consistent with Ni^{2+}, Co^{2+}, Sc^{3+}, and Sb^{5+} ions.

B. Magnetization measurements

Magnetic susceptibility (M/H) data for $Ni_{2-x}Co_xScSbO_6$ ($x = 0.1$, 0.2, 0.3 and 0.4) samples in a 1 T field are shown in Fig. S4 [24]. Sharp magnetic transitions at $T_C \approx 63$ K are observed for all samples, as also found for previous more Co rich samples [7]. Divergence of ZFC and FC data below T_C reveals that in addition to long range spin ordering, a glassy component is also present. This reflects the magnetic disorder

TABLE I. Magnetic parameters for $Ni_{2-x}Co_xScSbO_6$ ($x = 0.1$ to 0.4) materials. From susceptibility data: Weiss constant (θ), fitted (μ_{eff}) and spin-only theoretical (μ_{th}) effective paramagnetic moments; from *M*-*H* loops: critical field ($\mu_0 H_c$) and spontaneous magnetization (M_s, from extrapolation of M at high field to $H = 0$) at 1.5 K; from fits to zero field NPD data: ordered moment (m_s) and observed (obs.) k_z propagation vector from 1.5 K refinement; model (mo.) k_z values as decimals and $6/n$ fractions; and Curie temperature (T_C) and exponent (β) values from critical fits to ordered moment *vs* temperature plots.

x	0.1	0.2	0.3	0.4
θ (K)	−122	−124	−121	−117
μ_{eff} (μ_B)	4.87	5.13	5.27	5.38
$\mu_{th.}$ (μ_B)	4.22	4.44	4.65	4.85
$\mu_0 H_c$ (T)	2.45	2.51	2.49	2.35
M_s (μ_B)	0.16	0.19	0.26	0.25
m_s (μ_B)	1.79(2)	1.92(2)	2.02(2)	2.06(2)
k_z (obs.) (x 10^4)	760(3)	754(2)	731(2)	709(2)
k_z (mo.) (x 10^4)	759	750	732	706
k_z (mo.)	6/79	6/80	6/82	6/85
T_C (K)	62.6(1)	62.6(2)	63.6(2)	62.8(3)
β	0.22(1)	0.25(1)	0.23(1)	0.24(2)

resulting from the mixing of Ni/Co/Sc over three different cation sites as above. High temperature (>100 K) inverse ZFC data were fitted with a Curie-Weiss law, $\chi = C/(T-\theta)$, resulting in Weiss temperatures $\theta \approx -120$ K for all samples, implying strong antiferromagnetic exchange interactions that are moderately frustrated ($|\theta|/T_C \approx 2$) within and between the triangular spin layers in this corundum-related structure. The fitted paramagnetic moment increases with x, as expected for replacement of spin $S = 1$ Ni^{2+} by $S = 3/2$ Co^{2+}. The experimental values exceed the spin-only predictions by $0.5-0.6\,\mu_B$, which is consistent with an additional orbital contribution from Co^{2+} arising from spin-orbit coupling, but no clear variation with composition is seen over the limited substitution range studied. Parameters derived from magnetization and magnetic neutron diffraction data are shown in Table I.

Isothermal magnetization (*M*) - field (*H*) loops reveal metamagnetic transitions for all four $Ni_{2-x}Co_xScSbO_6$ samples. The measurements for $x = 0.1$ are shown in Fig. 2 and others are in Fig S5 [24]. A sharp (first order) metamagnetic transition is observed at lower temperatures (⟨50 K) in Fig. 2(a), but this becomes continuous (second order) approaching $T_C \approx$ 63 K in Fig. 2(b). The plot of metamagnetic critical field (H_c) in Fig. 2(c) shows an anomalous upturn at low temperatures which may reflect alignment of disordered spin components.

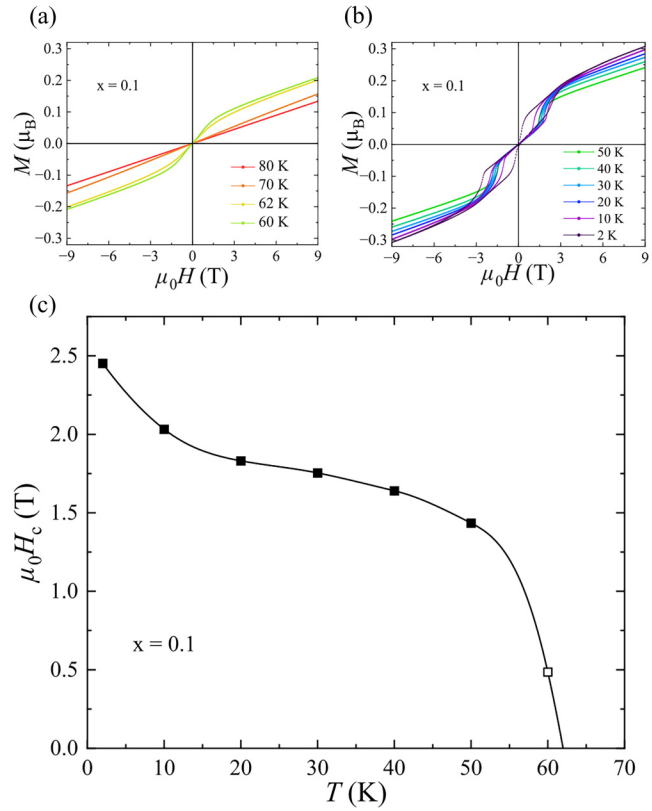


FIG. 2. Magnetization-field hysteresis loops for $x = 0.1$ at temperatures of (a) 60 to 80 K and (b) 2 to 50 K, showing the sharp metamagnetic transition in (b). (c) Temperature variation of the metamagnetic critical field from increasing field data (filled/open symbols = first/second order transition). The line is a guide to the eye.

C. Magnetic neutron diffraction

1. Zero field measurements

Prominent $\pm(101) + \boldsymbol{k}$ and $\pm(003) + \boldsymbol{k}$ magnetic satellite reflections with $\boldsymbol{k} = [0\,0\,k_z]$ are observed in neutron powder diffraction profiles from all of the $x = 0.1$ to 0.4 $Ni_{2-x}Co_xScSbO_6$ samples (Fig. S6) below 60 K ($\approx T_C$). Such magnetic satellites were previously reported for samples with $x \geqslant 0.5$ [7], and the same helical spiral model of ordered M1 and M2 site spins [Fig. 1(b)] was found to give good fits to the NPD data from base temperature up to T_C, as shown in Figs. 3 and S6 [24].

Plots of the ordered moment and lattice parameters from NPD fits against temperature (Figs. 4 and S8 [24]) reveal a strong coupling of spin order to the lattice. Strongly anisotropic cell parameter variations are observed where c shows negative thermal expansion below T_C while a and the overall volume expansion are positive but with anomalies below T_C.

This reveals a strong exchange striction in this layered system suggesting that magnetic frustration between spins in successive layers expands the interlayer separation while decreasing spin-spin separations within the *ab*-plane. Critical law fits to thermal variations of the ordered moment (Figs. 4 and S8) were used to derive precise values of the Curie temperature (T_C) and exponent β values as shown in Table I. Values of β are near to the theoretical value of 1/8 for Ising spins on a 2D lattice.

Refined values of k_z remain constant within error from base temperature until 60 K for each sample [Fig. 3(d)]. This would be surprising for a truly incommensurate spiral, where thermal variations in the balance between intra- and

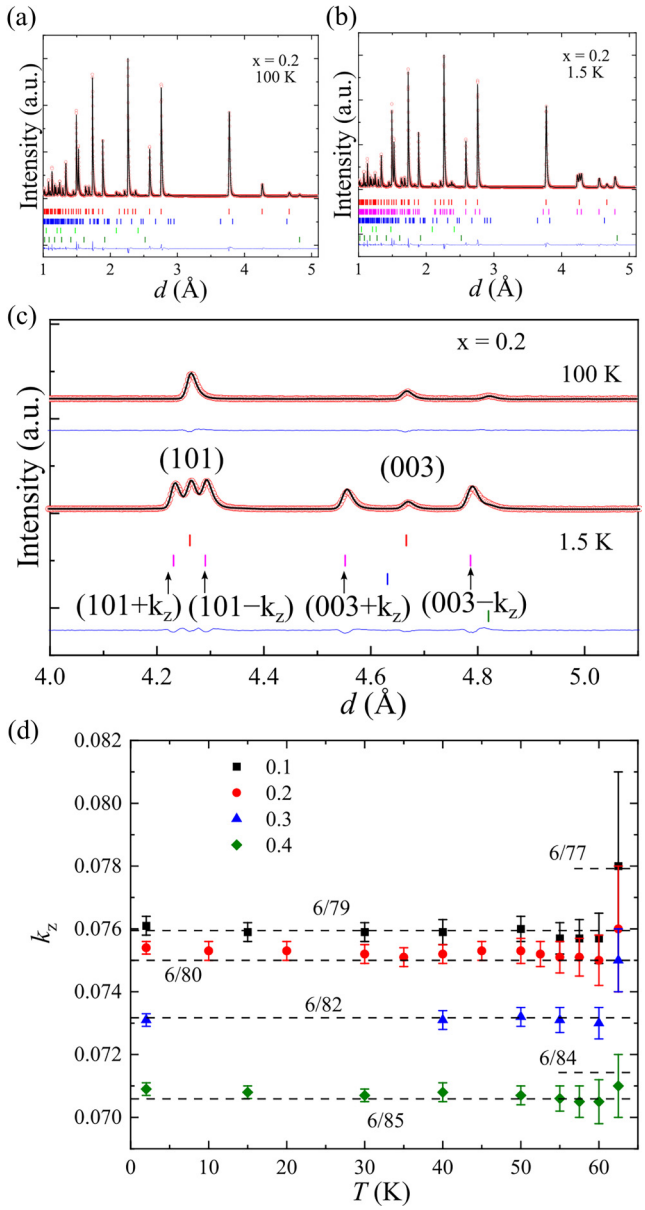


FIG. 3. (a) 100 K and (b) 1.5 K NPD Rietveld refinement plots for the $x = 0.2$ sample; red, purple, blue, light green, and dark green tick marks represent main phase $x = 0.2$ (97%), incommensurate $(00k_z)$ magnetic structure, $Sc_{5.5}Sb_{1.5}O_{12}$ (2%), NiO (1%), and NiO magnetic phase, respectively. The nuclear and magnetic reflections are listed. (c) Zoomed-in comparison of $x = 0.2$ NPD fits at 1.5 and 100 K, with magnetic satellites around (003) and (101) reflections labeled. (d) Thermal variations of k_z for the four $x = 0.1$ to 0.4 $Ni_{2-x}Co_xScSbO_6$ samples, showing model $6/n$ values.

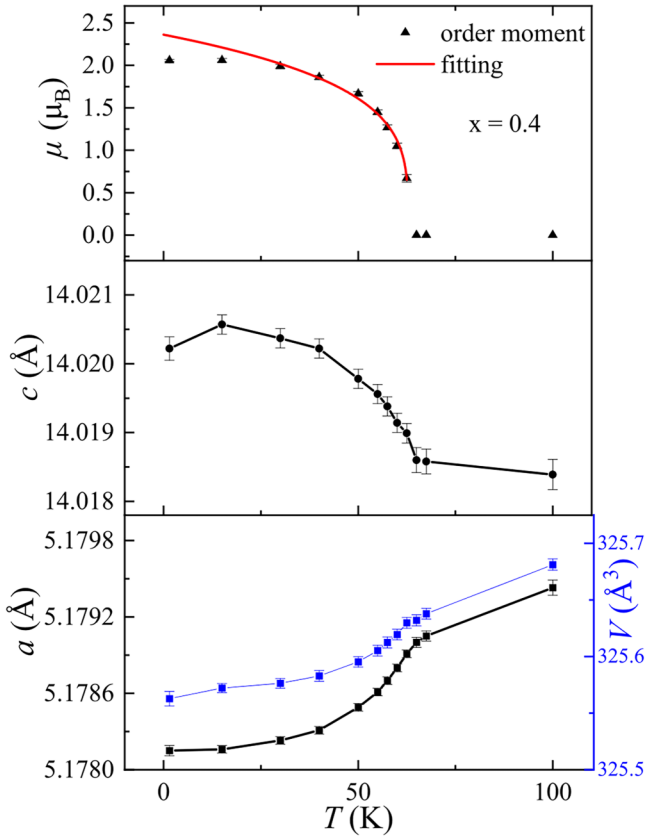


FIG. 4. Refined values of the ordered magnetic moment and cell parameters and volume from fits to neutron powder diffraction data for the $x = 0.2$ sample. Moment values are fit by the critical law $m(T) = m(0).[1 - (T/T_C)]^{\beta}$ in the $T_C/2 < T < T_C$ temperature region.

interplane exchange interactions arising from the anisotropic lattice expansion noted above would be expected to change wave vector. Such fixed k_z behavior is more consistent with locking-in of the helix, and although refined values of k_z in Table I do not take fractional $1/3n$ values as in previously reported samples [7], they can be assigned as fractional $6/n$ states, as discussed later. Further evidence for fractionalized behavior is that steps to another $k_z = 6/n$ state with smaller n are observed between 60 and 62 K, approaching $T_C \approx 63$ K. Clear steps; $k_z = 6/82 \rightarrow 6/80$ for $x = 0.3$, and $6/80 \rightarrow 6/79$ for $x = 0.2$; are seen in Fig. 3(d), although refinement errors become large approaching approaching T_C.

2. *Applied field measurements*

Neutron powder diffraction measurements carried out on $x = 0.1$ and 0.2 samples at constant temperatures (1.5 and 30 K) while increasing or decreasing magnetic field reveal changes in magnetic diffraction as shown in Fig. 5 for $x = 0.1$ and Fig. S9 [24] for $x = 0.2$. A clear change of magnetic diffraction is observed at the metamagnetic transition, principally the disappearance of the $\pm(003) + (00k_z)$ magnetic satellite reflections while the magnetic satellites in the vicinity of the (101) reflection shift and redistribute with field. This corresponds to a change from the helical spin structure with $\boldsymbol{k} = [0\,0\,k_z]$ observed at zero field [Fig. 1(b)] to a cycloidal structure with $\boldsymbol{k} = [k_x\,0\,0]$ propagation vector [Fig. 1(d)]. Moments rotate in the *ab*-plane in both magnetic structures. Both structures were refined as constant-magnitude circular spin rotations in the *ab*-plane. Similar *k*-flop transitions have been reported in other NTO types such as Ni_2InSbO_6 [25].

Weak $\pm(003) + 2\boldsymbol{k}$ magnetic satellites from the $\boldsymbol{k} = [0\,0\,k_z]$ helical phase are also observed as field increases up to 2 T and these disappear above the metamagnetic transition in the 2.5 T data (Figs. 5(b) and 5(c), S9 [24]). Such higher

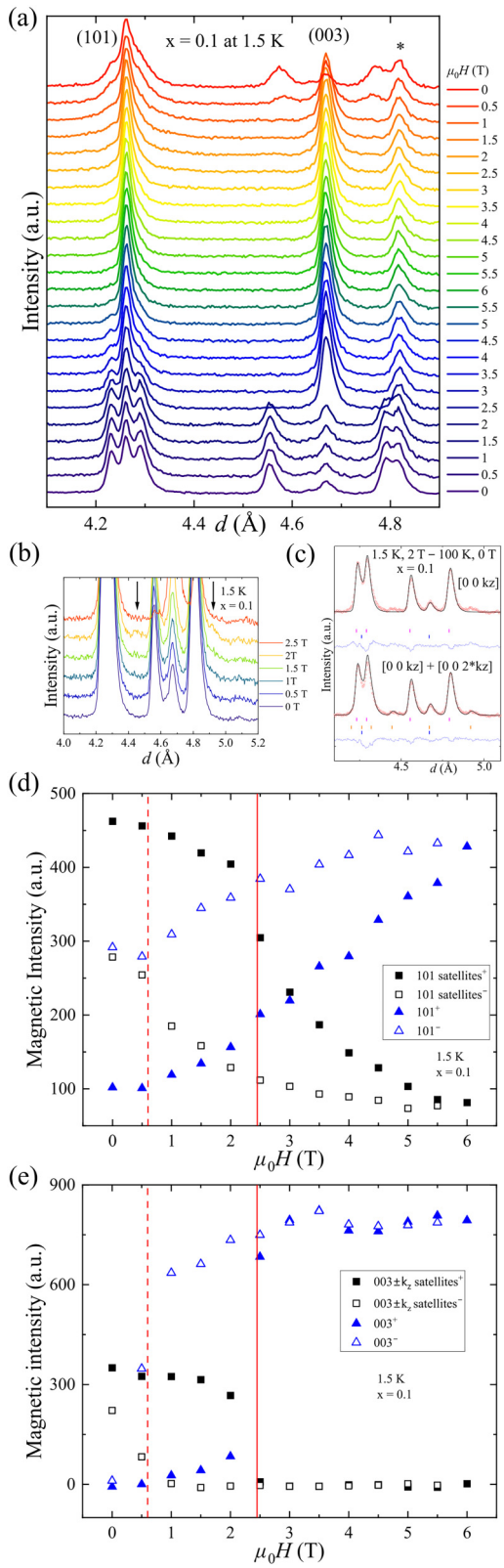


FIG. 5. Neutron powder diffraction data from the $x = 0.1$ sample at 1.5 K in applied magnetic fields. (a) The region showing prominent magnetic peaks as field increases from 0 (bottom) to 6 T and then decreases back to 0 (top). $\pm(003) + (00k_z)$ magnetic satellites at $d = 4.55$ and 4.78 Å disappear through the metamagnetic transition at 2.45 T in increasing field, and reappear in the reverse sweep below 0.6 T. A magnetic peak (*) from secondary phase NiO is observed at 4.85 Å. (b) Expanded data plot for increasing $0 \rightarrow 2.5$ T fields showing the appearance of weak $\pm(003) + 2\boldsymbol{k}$ magnetic satellites (arrowed) for $\boldsymbol{k} = [0\,0\,k_z]$ that grow up to 2 T but disappear above the metamagnetic transition at 2.5 T. (c) Fits to the data at 1.5 K and 2 T with 100 K in zero field data subtracted so that only magnetic contributions are seen. The upper fit is of Rietveld-calculated helical $\boldsymbol{k} = [0\,0\,k_z]$ and ferrimagnetic [0 0 0] phases (upper and lower Bragg markers) where $\pm(003) + 2\boldsymbol{k}$ satellites are seen as weak unfitted peaks. The lower fit adds fitting of these satellites using arbitrary peak intensities. (d) and (e) Magnetic peak intensities from the data shown in (a), obtained by subtracting the 100 K, zero field profile. 101 satellites refer to $(101 \pm k_z)$ below H_c and $(-1 \pm k_x 11)$ above H_c. 003 intensity includes overlapping satellites from $[k_x\,0\,0]$ above H_c. Intensities are shown as + (filled)/–(open) symbols for increasing/decreasing field in (d) and (e).

harmonics indicate that discommensurations (such as solitons) are introduced into the helical arrangement approaching the k-flop, but the $\pm(003) + 2\boldsymbol{k}$ satellite intensities are too weak to allow further quantitative analysis here.

Plots of magnetic peak intensity vs. field strength in Figs. 5(d) and 5(e) show that additional magnetic intensity develops at the nuclear (101) and (003) reflection positions with increasing field. The jump in intensity in the (003) region at the metamagnetic transition is due to the change from the helical $\boldsymbol{k} = [0\,0\,k_z]$ phase, which produces well-resolved $(003) \pm \boldsymbol{k}$ satellites, to the cycloidal $\boldsymbol{k} = [k_x\,0\,0]$ phase, for which the single $(003) \pm \boldsymbol{k}$ satellite is unresolved from the parent (003) reflection [Fig. 6(a)]. However, neither helimagnetic superstructure contributes at the nuclear (101) position, so the increase of magnetic intensity at this position reveals that another magnetic phase, identified as the ferrimagnetic $\boldsymbol{k} = [0\,0\,0]$ phase [Fig. 1(c)] is induced in the vicinity of the critical field. The variable field NPD data were thus fit using a $\boldsymbol{k} = [0\,0\,k_z]$ model at zero field, a mixture of $[0\,0\,k_z]$ and [0 0 0] magnetic phases at fields up to H_c, and coexisting $[k_x\,0\,0]$ and [0 0 0] phases above H_c. Fits are shown in Fig. 6(a) and S10 [24] and variations in the refined moment amplitudes are in Fig. 6(b). Ordered moments and magnetic phase fraction cannot be independently determined so the refined moments have been used to estimate magnetic phase proportions with the assumption that each phase has the same ordered moment. The evolution of the refined moment amplitudes shows a gradual redistribution of magnetic scattering from the incommensurate cycloidal component to the $\boldsymbol{k} = [0\,0\,0]$ phase with increasing field above H_c.

Refined values of k_x from all field dependent NPD data in Fig. 7 show that k_x decreases with increasing H. The values of k_x can be indexed by fractional $1/3n$ values although refinement errors in particular at higher fields and in decreasing field measurements are large in comparison to spacing of successive $1/3n$ state so the indexing is tentative. Steps that may be consistent with transitions between states in low increasing field data are evident, the clearest are from $k_x = 1/63$ at 2.5 and 3.0 T to $k_x = 1/66$ at 3.5 to 5.0 T with increasing H in Fig. 7(a). Neutron diffraction measurements on single crystals would be needed to measure more accurate k_x values and determine whether they correspond to fractional $1/3n$ states.

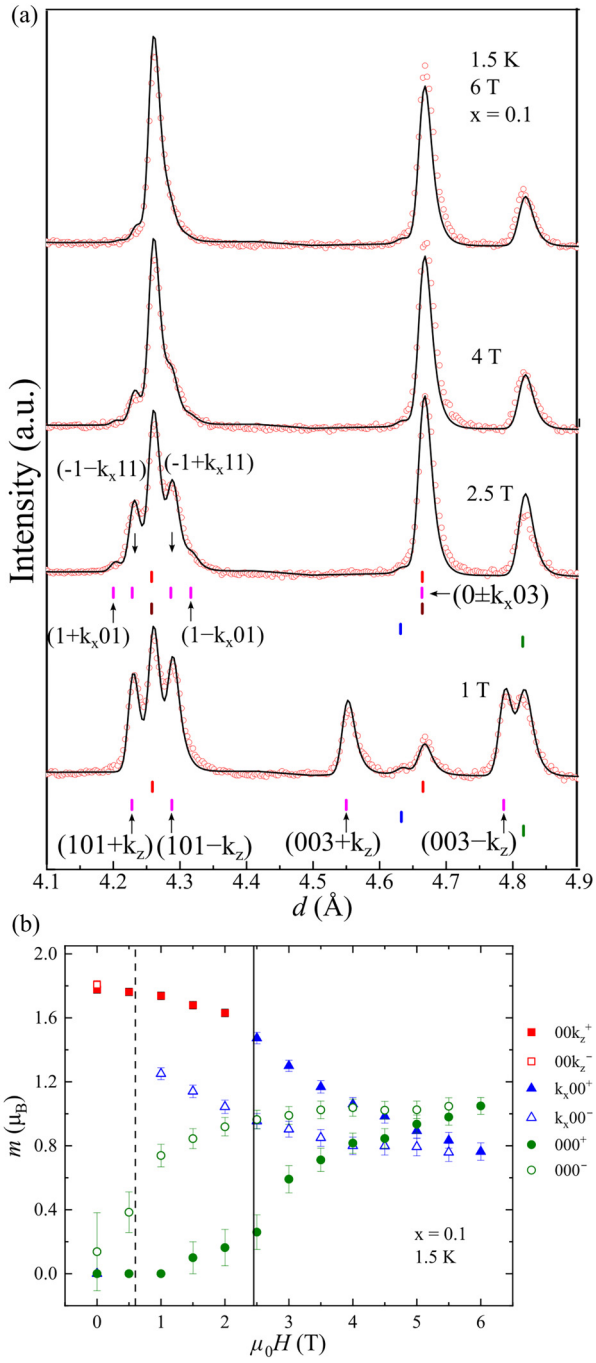


FIG. 6. (a) Rietveld fits to representative neutron diffraction profiles from Fig 5(a). Bragg markers (top to bottom) for 2.5 T fit are for nuclear $x = 0.1$, magnetic $[k_x\,0\,0]$ and $[0\,0\,0]$, $Sc_{5.5}Sb_{1.5}O_{12}$ impurity, and magnetic NiO phases; and for 1 T fit are for nuclear $x = 0.1$, magnetic $[0\,0\,k_z]$, $Sc_{5.5}Sb_{1.5}O_{12}$ impurity, and magnetic NiO phases. The $[k_x\,0\,0]$ and $[0\,0\,k_z]$ magnetic satellite reflections are indexed. $(-111) \pm k_x$ and $(0-11) \pm k_x$ satellites of the (101) reflection are degenerate in $d$spacing in the trigonal $R3$ power pattern. (b) Refined ordered-moment amplitudes for $[0\,0\,k_z]$, $[k_x\,0\,0]$, $[0\,0\,0]$ magnetic components of the $x = 0.1$ at 1.5 K. The magnetic components were refined using a common scale factor shared with the nuclear phase. Solid/dashed vertical lines mark the metamagnetic critical fields $\mu_0 H_c$ at 2.45/0.6 T for increasing/decreasing fields from magnetization data.

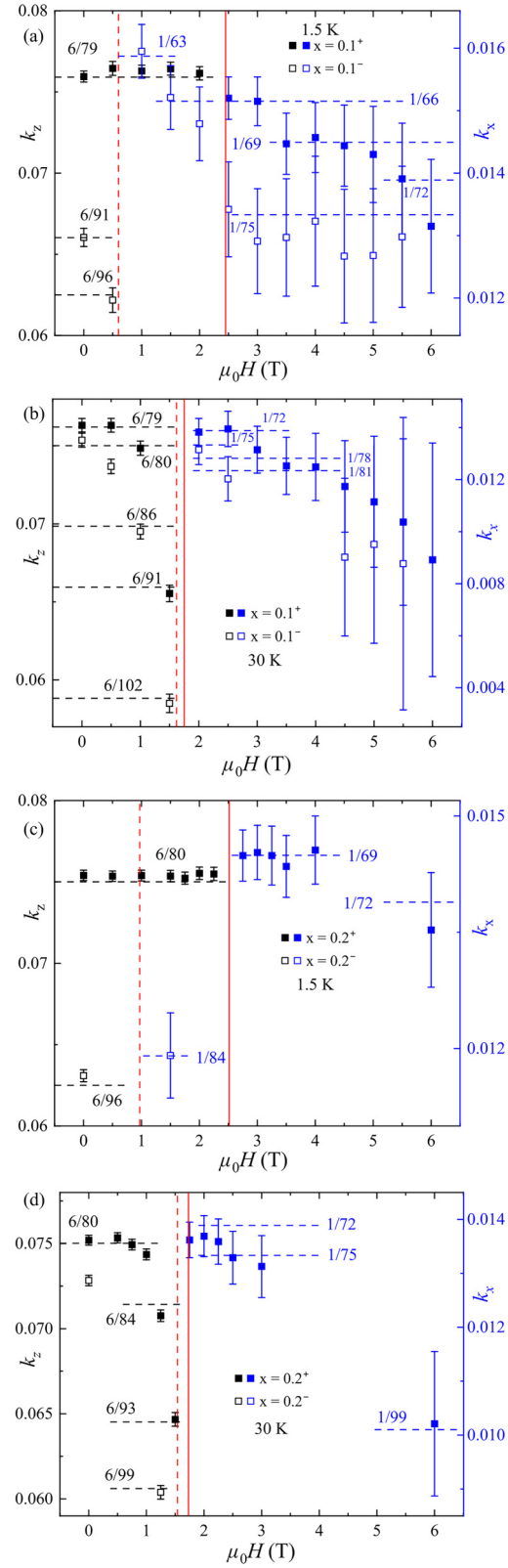


FIG. 7. Evolution of helical $[0\,0\,k_z]$ (black points, left scales) and cycloidal $[k_x\,0\,0]$ (blue points, right scales) wave vectors from fits to neutron powder diffraction data collected in increasing $0 \rightarrow 6$ T (filled points, + symbol) and decreasing $6\,\text{T} \rightarrow 0$ (open points, − symbol) magnetic fields. (a) $x = 0.1$ sample at 1.5 K. (b) $x = 0.1$ at 30 K. (c) $x = 0.2$ at 1.5 K. (d) $x = 0.2$ at 30 K. Error bars

IV. DISCUSSION

1. Magnetic phase diagram

A tentative $Ni_{2-x}Co_xScSbO_6$ magnetic phase diagram at base temperature is shown in Fig. 8(a). Present and previous [7] results demonstrate that the helical $[0\,0\,k_z]$ ground state exists almost completely across the series, from $x = 0.1$ to 2. The precise boundary between this and the $\boldsymbol{k} = [0\,0.036\,0]$ magnetic phase for $x = 0$ [18] has not yet been reported. The value of k_z decreases across the series, from 0.076 at $x = 0.1$ to 0.032 at $x = 2$.

Above the metamagnetic transition observed for $x = 0.1$ to 0.5 samples, the helical $[0\,0\,k_z]$ spin structure changes to a cycloidal $[k_x\,0\,0]$ arrangement with $k_x \sim 0.01$. This has only been characterised by NPD for $x = 0.1$ and 0.2 samples so far, so the high-field behavior of high-x compositions remains a future work.

Both the helical and cycloidal phases appear to be purely antiferromagnetic by neutron diffraction, with spins rotating in the *ab*-plane in both phases. However, they coexist with the ferrimagnetic $\boldsymbol{k} = [0\,0\,0]$ phase. Such coexistence likely reflects inhomogeneity within these complex, disordered materials which are difficult to prepare as fully phase-pure samples. The $\boldsymbol{k} = [0\,0\,0]$ phase is the k_x or $k_z \to 0$ limit of the spiral phases, and the proportion of [0 0 0] phase increases with H and with x. The present powder data do not distinguish uniquely whether the $\boldsymbol{k} = [0\,0\,0]$ contribution arises from separate ferrimagnetic domains or from a mixed-$\boldsymbol{k}$ state in which a uniform component is embedded within the k_x-type cycloidal domains, corresponding in the latter case to a fanlike field-induced structure.

A sharp metamagnetic transition is observed for low x [Figs. 2(a), 2(b), see also Fig. S5a] but appears to become more continuous and then is suppressed between $x = 0.5$ and 1.0. Magnetization jumps at metamagnetic transitions are often associated with spin-flop behavior. However, the magnetization jump at H_c appears to result from an abrupt increase in the proportion of the ferrimagnetic $\boldsymbol{k} = [0\,0\,0]$ phase accompanying the $[0\,0\,k_z] \to [k_x\,0\,0]$ transition, rather than from a simple spin-flop mechanism.

2. Magnetic staircases

Previously reported $x = 0.5$, 1.0, 1.5 and 2.0 samples were all found to adopt commensurate $k_z = 1/3n$ periodicities, evidencing strong locking to the lattice so that moments can lie parallel to threefold easy axes in the *ab*-plane. This gives six equivalent lowest-energy directions for moments to lie in, and some stabilization is gained by any commensurate $k = 6p/q$ wave vector (where p and q are integers), relative to nearby incommensurate values. This model corresponds to a complete devil's staircase that proceeds through an infinite number of commensurate states [4]. However, spirals locked into simple values of $6p/q$ such as $6/n$, $3/n$, $1/n$, $1/3n$, and $1/6n$ have greater easy-axis stabilization, and these may be used as 'harmless staircase' approximations, proceeding through finite numbers of commensurate states, to the complete devil's staircase. The previous $x = 0.5$, 1.0, 1.5, and 2.0 samples correspond to a harmless staircase of $k_z = 1/3n$ wave vectors, and the latter three samples all have $k_z = 1/6n$. The present $x = 0.1$, 0.2, 0.3 and 0.4 samples are more closely spaced in composition, and their wave vectors are described as a harmless staircase of $k_z = 6/n$ values.

It is difficult to distinguish a nontrivial commensurate wave vector such as $k_z = 6/n$ from an incommensurate wave vector, given uncertainties in experimental measurements, and hence to differentiate between a complete devil's staircase and the incomplete devil's staircase, with incommensurate periodicities between commensurate states. However, an experimental way to distinguish locked-in commensurate from incommensurate wave vectors is through their temperature

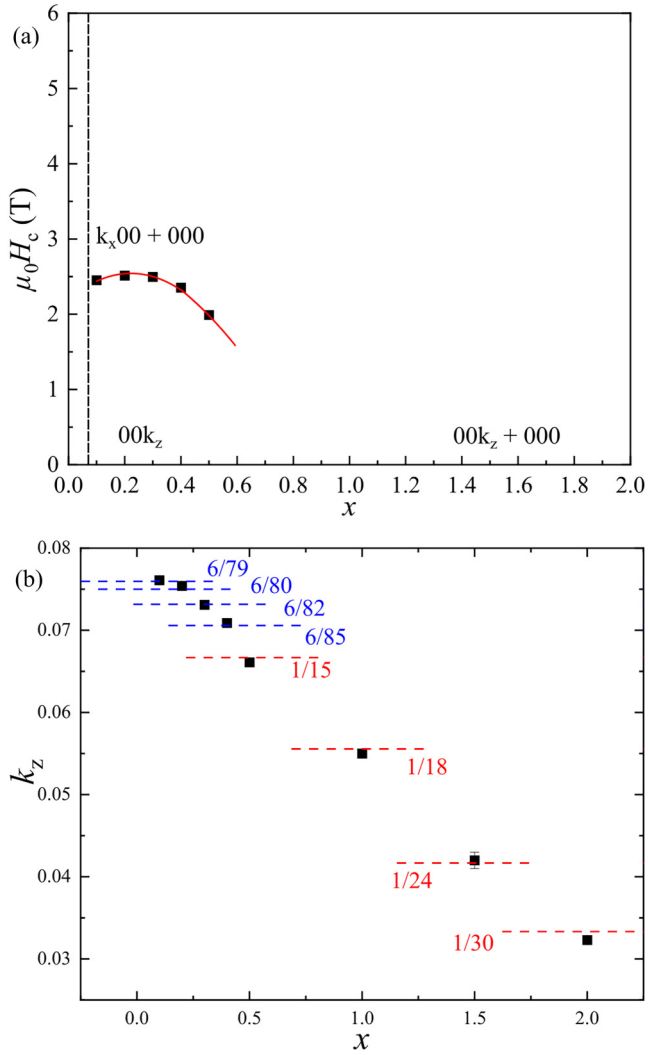


FIG. 8. (a) Phase diagram of $Ni_{2-x}Co_xScSbO_6$ at base temperature showing the metamagnetic transition from $[0\,0\,k_z]$ to $[k_x\,0\,0]$ spirals. (b) Variation of base temperature k_z with Co content showing fractional $1/3n$ (red) and $6/n$ (blue) values as a guide. Data are from this study and Ref. [7].

correspond to one e.s.d. (estimated standard deviation) from the fits and become large at high field as $\pm(101) + \boldsymbol{k}$ satellite intensities decrease. Fractional k values are shown as horizontal broken lines. Metamagnetic critical fields from magnetization measurements in increasing/decreasing field are shown as solid/broken vertical red lines.

dependence. Materials that adopt a magnetic spiral phase over a wide temperature range below the spin ordering transition typically show small systematic changes in k as the balance of frustrated magnetic interactions changes slightly. For example, the ilmenite-type polymorph of Mn_2CrSbO_6, which has a corundum-related structure similar to that of $Ni_{2-x}Co_xScSbO_6$, has a helical $\boldsymbol{k} = [0\,0\,k_z]$ spin structure that shows a smooth change from $k_z = 0.54$ at 2 K to $k_z = 0.46$ at 55 K, and with no lock-in plateaus at exact fractions such as $k_z = 1/2$, demonstrating that this is a genuinely incommensurate order [26]. Another (noncorundum) example is CrAs which adopts a helical $\boldsymbol{k} = [0\,0\,k_z]$ spin structure below Néel temperature $T_N = 267$ K, and the smooth increase from $k_z = 0.353$ at 2 K to $k_z = 0.381$ at 260 K, corresponding to an 8% change in k_z with no plateaus or other discontinuities, again shows that this is a genuinely incommensurate order [27]. In contrast, all four of the present $Ni_{2-x}Co_xScSbO_6$ samples have k_z close to $6/n$ values and showing no discernable change in k_z from 2 to 60 K to within $< 1\%$ refinement errors [Fig. 3(d)], despite anisotropic thermal lattice expansion that would be expected to shift the balance between frustrated magnetic exchange interactions. Small variations in k_z are observed in the temperature range 60–62 K approaching $T_C \approx 63$ K. These are consistent with steps between fractional values but as refinement errors are large in this region these assignments are tentative.

Variation of low temperature k_z values across the $Ni_{2-x}Co_xScSbO_6$ series based on present and previous samples is shown in Fig. 8(b). Studies of further samples at even smaller composition intervals will be needed to establish whether any of the fractional k_z states are stabilized for a significant range of x (a broad step), or whether the entire series evolves through a series of many locked-in narrow steps.

The field-dependent cycloidal k_x values shown in Fig. 7 decrease with increasing field and are compatible with fractional $1/3n$ values within experimental uncertainties, consistent with a possible staircaselike evolution, although this is tentative based on the present data. These results are also in keeping with the prediction [4] that hysteresis effects should be observable in harmless (and complete devil's) staircases, although experimental uncertainties in k_x values at high and reversing fields are large. It is also notable that, unlike in the zero-field $[0\,0\,k_z]$ helices, the cycloidal $[k_x\,0\,0]$ wave vectors show clear changes with temperature, e.g. from apparent $k_x = 1/66$ at 1.5 K to 1/72 at 30 K for the x = 0.1 sample in a 2.5 T field [Figs. 7(a) and 7(b)]. Hence, further experiments to follow temperature dependence of k_x at a constant high field may be valuable in demonstrating staircase variation.

In summary, there is strong evidence that magnetic spirals in $Ni_{2-x}Co_xScSbO_6$ exemplify complete devil's staircase behavior. Unlike the canonical rare earth based systems [5–6] where thermal steps in wave vector provide principal evidence for staircase behavior, strong locking in of moments in $Ni_{2-x}Co_xScSbO_6$ results in helical $[0\,0\,k_z]$ wave vectors that show little thermal variation except when very close to T_C, and chemical variation of x is the primary tuning parameter. However, fractional steps in high-field cycloidal $[k_x\,0\,0]$ wave vectors with changing field or temperature are more apparent. Further investigations of the x, T, and H dependence of the spin spirals will be needed to explore their fractionalized variations. As these NTO-type materials are also acentric, chiral and polar, then couplings of the magnetic states to electrical polarization could also be explored.

V. CONCLUSIONS

Studies of lightly cobalt doped $Ni_{2-x}Co_xScSbO_6$ samples ($x = 0.1$ to 0.4) have shown that all adopt a helical $[0\,0\,k_z]$ magnetic ground state below $T_C \approx 63$ K. Metamagnetic transitions in applied magnetic fields of ~ 2.5 T mark a k-flop from helical $\boldsymbol{k} = [0\,0\,k_z]$ to cycloidal $\boldsymbol{k} = [k_x\,0\,0]$ spin spirals, and the latter gradually transforms to a coexisting ferrimagnetic $\boldsymbol{k} = [0\,0\,0]$ state at higher field. Fractional values of k_z and k_x are consistent with complete devil's staircase behavior, driven by locking-in of spins to easy-axis directions in the ab-plane that stabilizes commensurate $6p/q$ wave vectors.

ACKNOWLEDGMENTS

The authors thank EPSRC for financial support of this research through project EP/P021786/1. We are also grateful to Science and Technology Facilities Council (STFC) for ISIS beamtime allocation on the WISH instrument.

DATA AVAILABILITY

The data that support the findings of this article are openly available [28].

[1] N. A. Hill, Why are there so few magnetic ferroelectrics? J. Phys. Chem. B **104**, 6694 (2000).
[2] M. Fiebig, Revival of the magnetoelectric effect, J. Phys. D **38**, R123 (2005).
[3] J. F. Scott, Multiferroic memories, Nat. Mater. **6**, 256 (2007).
[4] P. Bak, Commensurate phases, incommensurate phases and the devil's staircase, Rep. Prog. Phys. **45**, 587 (1982).
[5] D. Gibbs, D. E. Moncton, K. L. D'Amico, J. Bohr, and B. H. Grier, Magnetic x-ray scattering studies of holmium using synchro-tron radiation, Phys. Rev. Lett. **55**, 234 (1985).
[6] P. Fischer, G. Meier, B. Lebech, B. D. Rainford, and O. Vogt, Magnetic phase transitions of CeSb. I. Zero applied magnetic field, J. Phys. C: Solid State Phys. **11**, 345 (1978).
[7] K. Ji, E. Solana-Madruga, A. M. Arevalo-Lopez, P. Manuel, C. Ritter, A. Senyshyn, and J. P. Attfield, Lock-in spin structures and ferrimagnetism in polar $Ni_{2-x}Co_xScSbO_6$ oxides, Chem. Commun. **54**, 12523 (2018).
[8] W. Eerenstein, N. D. Mathur, and J. F. Scott, Multiferroic and magnetoelectric materials, Nature (London) **442**, 759 (2006).
[9] S.-W. Cheong and M. Mostovoy, Multiferroics: A magnetic twist for ferroelectricity, Nat. Mater. **6**, 13 (2007).
[10] Y. S. Oh, S. Artyukhin, J. J. Yang, V. Zapf, J. W. Kim, D. Vanderbilt, and S.-W. Cheong, Non-hysteretic colossal magnetoelectricity in a collinear antiferromagnet, Nat. Commun. **5**, 3201 (2014).

[11] J. W. Kim, S. Artyukhin, E. D. Mun, M. Jaime, N. Harrison, A. Hansen, J. J. Yang, Y. S. Oh, D. Vanderbilt, V. S. Zapf, and S.-W. Cheong, Successive magnetic-field-induced transitions and colossal magnetoelectric effect in Ni_3TeO_6, Phys. Rev. Lett. **115**, 137201 (2015).

[12] G. H. Cai, M. Greenblatt, and M. R. Li, Polar magnets in double corundum oxides, Chem. Mater. **29**, 5447 (2017).

[13] L. I. Kosse, E. D. Politova, V. V. Chechkin, E. A. Myzgin, Y. N. Medvedev, and B. S. Venevtsev, Ferroelectric properties of compounds with the magnesium orthotellurate structure, Izv. Akad. Nauk SSSR Neorg. Mater. (USSR) **18**, 1879 (1982).

[14] L. I. Kosse, E. D. Politova, and Y. N. Venevtsev, Structural, field, and dielectric properties of compounds with the magnesium orthotellurate structure, Zh. Neorg. Khim. (USSR) **28**, 1689 (1983).

[15] N. A. Hill and A. Filippetti, Why are there any magnetic ferroelectrics? J. Magn. Magn. Mater. **242–245**, 976 (2002).

[16] D. I. Khomskii, Classifying multiferroics: Mechanisms and effects, Physics Magazine **2**, 20 (2009).

[17] M.-R. Li, M. Croft, P. W. Stephens, M. Ye, D. Vanderbilt, M. Retuerto, Z. Deng, C. P. Grams, J. Hemberger, J. Hadermann, W.-M. Li, C.-Q. Jin, F. O. Saouma, J. I. Jang, H. Akamatsu, V. Gopalan, D. Walker, and M. Greenblatt, Mn_2FeWO_6: A new Ni_3TeO_6-type polar and magnetic oxide, Adv. Mater. **27**, 2177 (2015).

[18] S. A. Ivanov, R. Mathieu, P. Nordblad, R. Tellgren, C. Ritter, E. Politova, G. Kaleva, A. Mosunov, S. Stefanovich, and M. Weil, Spin and dipole ordering in Ni_2InSbO_6 and Ni_2ScSbO_6 with corundum-related structure, Chem. Mater. **25**, 935 (2013).

[19] A. M. Arevalo-Lopez, E. Solana-Madruga, E. P Arevalo-Lopez, A. J. Dos Santos-García, D. Avila-Brande, C. Ritter, J. P. Attfield, and R. Saez-Puche, High pressure synthesis of polar and non-polar cation-ordered polymorphs of Mn_2ScSbO_6, Dalton Trans. **44**, 20441 (2015).

[20] Á. M. Arévalo-López, E. Solana-Madruga, E. P. Arévalo-López, D. Khalyavin, M. Kepa, A. J. Dos Santos-García, and J. P. Attfield, Evolving spin periodicity and lock-in transition in the frustrated ordered ilmenite-type $\beta-Mn_2InSbO_6$, Phys. Rev. B **98**, 214403 (2018).

[21] M. Li, E. E. McCabe, P. W. Stephens, *et al.*, Magnetostriction-polarization coupling in multiferroic Mn_2MnWO_6, Nat. Commun. **8**, 2037 (2017).

[22] J. Rodriguez-Carvajal, Recent advances in magnetic structure determination by neutron powder diffraction, Physica B **192**, 55 (1993).

[23] J. Rodriguez-Carvajal, BASIREPS: a program for calculating irreducible representations of space groups and basis functions for axial and polar vector properties. Part of the FullProf Suite of programs available at http://www.ill.eu/sites/fullprof/.

[24] See Supplemental Material at http://link.aps.org/supplemental/10.1103/dlvy-9bd9 for further plots and fits to magnetization and neutron diffraction data, and for tables of crystallographic parameters and magnetic representations.

[25] Y. Ihara, R. Hiyoshi, M. Shimohashi, R. Kumar, T. Sasaki, M. Hirata, Y. Araki, Y. Tokunaga, and T. Arima, Field-induced magnetic structures in the chiral polar antiferromagnet Ni_2InSbO_6, Phys. Rev. B **108**, 024417 (2023).

[26] A. J. Dos Santos-García, E. Solana-Madruga, C. Ritter, D. Ávila-Brande, O. Fabelo, and R. Sáez-Puche, Synthesis, structures and magnetic properties of the dimorphic Mn_2CrSbO_6 oxide, Dalton Trans. **44**, 10665 (2015).

[27] A. Eich, A. Grzechnik, Y. Su, B. Ouladdiaf, D. Sheptyakov, T. Wolf, V. Petríček, H. Shahed, and K. Friese, Incommensurate magnetic structure of CrAs at low temperatures and high pressures, Acta Cryst. B **79**, 473 (2023).

[28] J. P. Attfield and K. Ji [Edinburgh DataShare], https://doi.org/10.7488/ds/8113 (2026).